Combustion Theory and Modelling
Vol. 11, No. 3, June 2007, 351–376

Taylor & Francis
Taylor & Francis Group

A numerical study of auto-ignition in turbulent lifted flames issuing into a vitiated co-flow

R. L. GORDON*†, A. R. MASRI†, S. B. POPE‡ and G. M. GOLDIN§

†School of Aerospace, Mechanical and Mechatronic Engineering, The University of Sydney, NSW 2006, Australia
‡Mechanical and Aerospace Engineering, Cornell University, Ithaca, NY 14853, USA
§Fluent Inc, Lebanon, New Hampshire, USA

(Received 8 August 2005)

This paper presents a numerical study of auto-ignition in simple jets of a hydrogen–nitrogen mixture issuing into a vitiated co-flowing stream. The stabilization region of these flames is complex and, depending on the flow conditions, may undergo a transition from auto-ignition to premixed flame propagation. The objective of this paper is to develop numerical indicators for identifying such behavior, first in well-known simple test cases and then in the lifted turbulent flames. The calculations employ a composition probability density function (PDF) approach coupled to the commercial CFD code, FLUENT. The in-situ-adaptive tabulation (ISAT) method is used to implement detailed chemical kinetics. A simple k–ε turbulence model is used for turbulence along with a low Reynolds number model close to the solid walls of the fuel pipe.

The first indicator is based on an analysis of the species transport with respect to the budget of convection, diffusion and chemical reaction terms. This is a powerful tool for investigating aspects of turbulent combustion that would otherwise be prohibitive or impossible to examine experimentally. Reaction balanced by convection with minimal axial diffusion is taken as an indicator of auto-ignition while a diffusive–reactive balance, preceded by a convective–diffusive balanced pre-heat zone, is representative of a premixed flame. The second indicator is the relative location of the onset of creation of certain radical species such as HO_2 ahead of the flame zone. The buildup of HO_2 prior to the creation of H, O and OH is taken as another indicator of autoignition.

The paper first confirms the relevance of these indicators with respect to two simple test cases representing clear auto-ignition and premixed flame propagation. Three turbulent lifted flames are then investigated and the presence of auto-ignition is identified. These numerical tools are essential in providing valuable insights into the stabilization behaviour of these flames, and the demarcation between processes of auto-ignition and premixed flame propagation.

Keywords: Turbulent; Non-premixed flames; Lifted flames; Auto-ignition

1. Introduction

A long-term objective of combustion research is to develop computational models that may be used as engineering tools to optimize combustor designs. Such a goal is gradually approached through the development of improved physical sub-models, more efficient numerical algorithms and enhanced representations of detailed chemical kinetics. This process should involve regular comparisons with established databases that help validate relevant

*Corresponding author. E-mail: robert.gordon@aeromech.usyd.edu.au

Combustion Theory and Modelling
ISSN: 1364-7830 (print), 1741-3559 (online)
http://www.tandf.co.uk/journals
DOI: 10.1080/13647830600903472

aspects of the models. The particle-based probability density function (PDF) approach is one of the methodologies already making significant advances in this field. It has already been demonstrated to have the capability to employ detailed chemical kinetics to compute the structure of flames that are undergoing significant local extinction and re-ignition [1–3]. With computational cost being intermediate between Reynolds averaged approaches (RANS) and large eddy simulations (LES), PDF methods are gradually expanding their range of applicability into combustion environments that are either fluid-dynamically more complex such as recirculating [4] and swirling flows [5] or involve more subtle chemical kinetics such as auto-ignition processes [6, 7].

One issue that has been somewhat under-exploited in the development process of advanced numerical methods in combustion is the potential to employ these tools to enhance our understanding of specific aspects of the combustion process. These 'numerical experiments', the likes of which are common to users of direct numerical stimulation (DNS), would be extremely useful especially in situations where actual experiments or direct simulations are very expensive or not possible. A typical scenario, investigated in this paper, is the understanding of auto-ignition processes that may exist at the base of lifted flames issuing in a vitiated co-flow [8, 9]. Flame stabilization through partially premixed flame propagation may also be of importance in this region of the flow so this phenomenon is also explored in the calculations. It should be emphasized here that numerical experiments should be restricted to issues where the computations may be done with a high level of numerical accuracy.

Auto-ignition is relevant to many combustion engineering applications, such as diesel engines and lean premixed combustors. This process is complex owing to its strong dependence on chemical kinetics as well as fluid dynamics. Numerical and theoretical studies of auto-ignition [10–19] have shown that mixtures do not necessarily ignite at stoichiometric conditions but rather at mixture fractions where the fluid is most reactive yet the scalar dissipation rate is relatively low. While direct numerical simulations are proving to be extremely useful tools in furthering current understanding of auto-ignition [12–14, 17–19], they remain impractically expensive for the high Reynolds number cases considered here. In an earlier paper, the PDF approach has been used to make computations of the structure of a turbulent flame of H_2/N_2 fuel issuing in a vitiated co-flow [6]. Numerical and modeling issues were thoroughly investigated and the calculations compared favourably with measurements. As the level of confidence increases in such computations, further numerical experiments may then be conducted to explore issues of auto-ignition and lifted flame stabilization.

This paper focuses on the issue of auto-ignition and attempts to develop a set of indicators that characterize the occurrence of this phenomenon and differentiate it from, say, premixed flame propagation. Two approaches are explored here: the first compares the budgets of the turbulent diffusive, mean-flow convective and chemical reaction processes in the region of flame stabilization; the second investigates the 'time history' ahead of the reaction zone of radicals such as H and HO_2. These indicators are tested and validated in simple model problems and then applied to three turbulent lifted flames issuing in co-flowing streams of different temperatures. Similar concepts have been investigated for a detached laminar flame in the two-dimensional (2D) DNS of [19].

2. Model description

2.1 *The burner*

Figures 1(a) and 1(b) show, respectively, a schematic of the burner and the computational domains used in the current calculations. The fuel jet, which has an inner diameter $D = 4.57$ mm

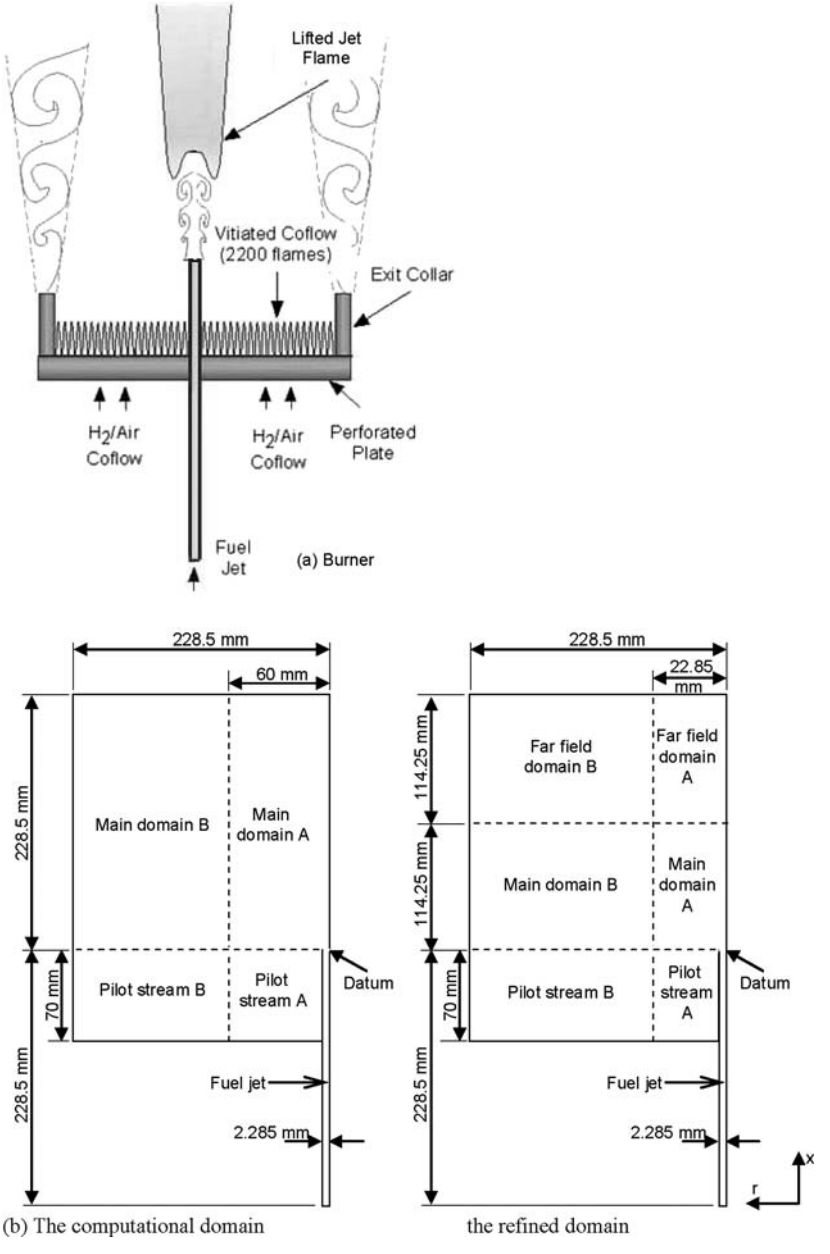

Figure 1. (a) Schematic of the burner, showing the perforated coflow plate and fuel jet tube extending into the vitiated coflow stream, and (b) standard (29 707 orthogonal cells) and refined (50 875 orthogonal cells) computational domains. The main domain A region in the refined domain (RHS) is meshed with cells of uniform spacing.

and a wall thickness of 0.89 mm, is located at the centre of a perforated disk with a diameter of 210 mm. The disk has 2200 $\times$ 1.58 mm diameter holes which stabilize as many premixed flames, providing a hot co-flowing stream. The overall blockage of the perforated plate is 87%. The central fuel jet extends by 70 mm downstream of the surface of the perforated plate so that the fuel mixture exits in a co-flow of nearly uniform composition. The entire burner

Table 1. Flame and flow conditions.

Central jet		Co-flow	
T_{jet} (K)	305	T_{coflow} (K)	1045
V_{jet} (m/s)	107	V_{coflow} (m/s)	3.5
Re_{jet}	23,600	Re_{coflow}	2,500
f_{stoich}	0.47	Φ	0.25
X_{H2}	0.25	X_{O2}	0.1474
X_{N2}	0.75	X_{H2O}	0.0989
		X_{N2}	0.7534

assembly is shrouded with a water jacket for cooling, and sits in stagnant air. The base flame modelled is that of Cabra *et al.* [8]. The conditions for this flame are given in table 1.

2.2 *The code*

All computations presented here use the FLUENT 6.2 code that solves RANS equations for the mean conservation of mass, momentum and energy, together with the k–ε turbulence model equations. A modelled transport equation for the composition PDF is coupled and solved using a Lagrangian particle-based Monte Carlo method. In the flows considered here, the density computed from the thermochemical field is consistent with that computed from the flow field as this constitutes the only feedback from the PDF to the RANS section of the code. Modified Curl (MC) is used as the mixing model. A full list of the numerical conditions is detailed in table 2.

The chemical mechanism used is developed by Mueller *et al*. [20] and involves ten species (H_2, H, O, O_2, OH, H_2O, HO_2, H_2O_2, Ar, N_2) and 21 reactions. This is incorporated in the PDF method using the in-situ-adaptive tabulation (ISAT) algorithm developed by Pope [21].

The origin of the co-ordinate system is taken at the centre of the jet exit plane. The computational domain is also shown in figure 1(b) and extends in the co-flowing stream from the face of the pilot plate to 50 jet diameters downstream (x = 228.5 mm). Computations in the fuel line are initiated some 50 jet diameters upstream of the exit plane (x = −228.5 mm to +228.5 mm). The domain also extends radially out from the centreline to 50 jet diameters (from r = 0 to 228.5 mm).

Numerically accurate calculations are ensured here by adopting, as a baseline, the optimized numerical conditions of Masri *et al.* [6] who used 20 particles per cell, an ISAT error tolerance of 6.25×10^{-6}, and an ODE error tolerance of 1.0×10^{-8}. This is justified considering that the current calculations employ the same computational domain and numerical schemes.

Table 2. Numerical conditions selected for computing the jet and flame in a vitiated co-flow.

Domain	Axisymmetric
Solver	Steady, segregated with implicit formulation
Turbulence model	Standard k-ε with $C_\mu = 0.09$, $C_{\varepsilon 1} = 1.44$, $C_{\varepsilon 2} = 1.92$, $\sigma_k = 1.0$, $\sigma_\varepsilon = 1.3$, $\sigma_\Phi = 0.7$
Mixing model	Modified curl, $C_\phi = 2.0$
Wall treatment	Low Reynolds number model
Discretization schemes	Presto for pressure PISO for pressure–velocity coupling Second order upwind for momentum and turbulent kinetic energy
Under-relaxation factors	Pressure = 0.3, density = 1.0, body forces = 1.0, momentum = 0.7
Local time stepping	Courant number = 0.5

Table 3. Details of the standard domain mesh.

	x		r		Mesh Cells	
	From (mm)	To (mm)	From (mm)	To (mm)	x	r
Fuel jet	−228.5	0	0	2.285	108	20
Pilot stream A	−70	0	2.285	60	44	124
Pilot stream B	−70	0	60	228.5	44	28
Main domain A	0	228.5	0	60	152	∼ 76
Main domain B	0	228.5	60	228.5	152	∼ 62
Total cells					29 707	

2.3 *Boundary and grid conditions*

Grid independence studies performed by Masri *et al.* [6] resulted in an optimal non-uniform mesh consisting of 29 707 cells. This mesh, described in table 3, was used here to conduct a parametric study of the flame. A finer grid (table 4), with uniform cell spacing throughout the ignition region, was also used with 50 particles per cell for the calculation of the species transport budget terms.

The boundary conditions are also identical with those of Masri *et al.* [6] except that a turbulent kinetic energy, k, of 200 m^2/s^2 and a dissipation rate, ε, of 100 000 $m^2/s^3$are used for the fuel inlet. These were used to approximate an integral length scale of 4.57 mm which is equivalent to the fuel jet diameter. The turbulence intensity was set at ∼10% but it is worth noting that the solution is found to be insensitive to the turbulence levels at the exit plane. The solution domain, shown in figure 1(b), is axisymmetric about the x axis and r is used to denote the radial coordinate. Conjugate heat transfer across the steel fuel tube is accounted for in the calculations. The tube is modelled as a 0.89 mm thick steel wall, with a density of 8030 kg/m^3, specific heat $C_p = 502.48$ J/kgK, and a thermal conductivity calculated piecewise-linearly over the values in table 5.

The refined mesh cases were calculated with the parallel version of FLUENT across 32 Intel Xeon processors, each with 2.4 MHz and 1 Gb of RAM. For the turbulent flame case with 50 875 cells and 50 particles per cell, the average time per iteration is slightly over 2 min.

2.4 *The test cases*

Two simple test cases are used here for validation: (a) a one-dimensional (1D) plug flow reactor for simulating auto-ignition and (b) a 2D counterflow premixed flame. The physical

Table 4. Details of the refined domain mesh.

	X		r		Mesh Cells	
	From (mm)	To (mm)	From (mm)	To (mm)	x	r
Fuel jet	−228.5	0	0	2.285	140	15
Pilot stream A	−70	0	2.285	22.85	40	50
Pilot stream B	−70	0	22.85	228.5	40	60
Main domain A	0	114.25	0	22.85	300	65
Main domain B	0	114.25	22.85	228.5	300	60
Far field domain A	114.25	228.5	0	22.85	55	65
Far field domain B	114.25	228.5	22.85	228.5	55	60
Total cells					50 875	

Table 5. Thermal conductivity of steel at various temperatures [22].

Temperature	Thermal conductivity
300 K	13.4 W/m K
400 K	15.2 W/m K
600 K	18.3 W/m K

sub-models and the numerical parameters employed here are identical with those used in the turbulent lifted flame calculations, except that 100 particles per cell are used for these cases. The plug flow reactor domain is 1 m long, 1 cm wide, and is divided into a single row of 1000 equal-sized cells. Inlet conditions are detailed in table 6.

This composition is representative of a mixture fraction of 0.2 from the lifted flame case with a co-flow temperature of 1045 K, corresponding to the conditions just within the ignition zone. The temperature has been elevated from the mixture temperature of 897 K, however, to reduce the ignition delay for this test case. Tests of this mixture using CHEMKIN with full chemistry give an autoignition delay of 8.8×10^{-3} s. This test case exhibits an autoignition delay of 9.2×10^{-3} s when k is set to 1 m^2/s^2 and ε set to 1 m^2/s^3, and a reduced delay of 6×10^{-3} s under the turbulence conditions stated above. An empirical expression for the ignition delay of hydrogen–oxygen mixtures from [23] gives a delay of 8×10^{-3} s. The adiabatic temperature of 1442.4 K is consistent with the CHEMKIN calculation of 1442.8 K.

The counterflow premixed case consists of a 2 cm by 1 cm domain with a 100×50 cell uniform mesh. A schematic of the domain is shown in figure 2. The flame is stabilized close to the stagnation plane by a counterflow of combustion products at equilibrium composition and the adiabatic flame temperature. The boundary conditions are given in table 7. The cold fuel inlet mixture is stoichiometric for a humid air–hydrogen mixture. Data are taken along the symmetry boundary to approximate a 1D premixed flame.

When using the k–ε turbulence model, boundary conditions are required for the turbulent kinetic energy, k, and the turbulence dissipation rate, ε. For this case, these are calculated from the values for the turbulence intensity, I, and the large-eddy (or Integral) length scale l given in table 6 (above). Equations (1) and (2) give the boundary condition for k

$$\mathrm{k} = \frac{3}{2}(u')^2 \tag{1}$$

$$u' = I \times \bar{u} \tag{2}$$

Table 6. Inlet boundary conditions for the 1D plug flow reactor.

	Inlet condition
Property	
Velocity	100 m/s
Temperature	1003 K
k	200 m^2/s^2
ϵ	100 000 m^2/s^3
Composition (mass fraction)	
H_2	0.004688
O_2	0.136703
H_2O	0.051640
N_2	Balance

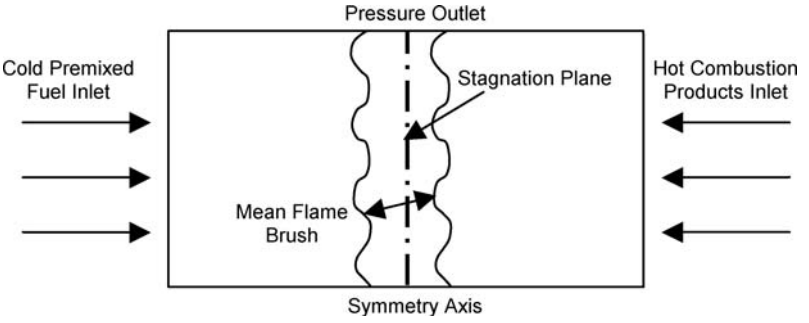

Figure 2. Domain of the counterflow premixed burner. The flame is stabilized close to the stagnation plane by a counter flow of gases at the adiabatic flame temperature of the fuel and of equilibrium composition.

where $\bar{u}$ is the mean inlet velocity, u' is an approximate velocity fluctuation. I is here specified as 10%. The boundary condition for ε is given by equation (3)

$$\varepsilon = (C_\mu)^{3/4} \times \frac{(\mathrm{k})^{3/4}}{l} \tag{3}$$

where C_μ is a constant, given in table 1 (0.09), and l is a length scale set to 0.1 mm as shown in table 6. The flame width decreases with decreasing turbulence length scale for this case, so scales varying from 10 mm to 0.1 mm were tested, with 0.1 mm chosen to give a flame brush sufficiently removed from the inlet boundaries.

2.5 *Time averaging*

Two methods of averaging are combined in PDF–RANS calculations: mass-weighted averaging over the ensemble of PDF particles within each cell; and pseudo time averaging of the solution over a number of iterations (once the statistically stationary state has been reached). For most scalars, reasonably smooth mean composition fields may be attained with a number of iterations in the time average (hereafter N_{TA}) of around 100 to 250 and number of particles per cell (N_{PC}) of 20 to 30. However, in the present case the diffusion fields are calculated from

Table 7. Boundary conditions for counterflow premixed burner.

	Cold inlet	Hot inlet
Velocity	0.5 m/s	1.5 m/s
Temperature	300 K	1364.8 K
Turbulence intensity, I	10%	10%
Integral length scale, l	0.0001 m	0.0001 m
Composition (mass fraction)		
H_2	0.01122	7.62×10^{-7}
O_2	0.08907	3.14×10^{-5}
H_2O	0.03365	0.13391
H		3.57×10^{-10}
O		1.82×10^{-9}
OH		2.1×10^{-6}
HO_2		1.67×10^{-10}
H_2O_2		1.09×10^{-10}
Ar	0.01	0
N_2	Balance	Balance

the second derivatives of the mean composition fields and hence are extremely sensitive to small fluctuations. This requires that averaging be performed over significantly larger values for both N_{TA} and N_{PC} to improve the quality of the results.

The error between the estimated mean and the true mean may be written

$$E = \frac{b}{N_{PC}} + \frac{c \times \xi}{\sqrt{N_{PC} N_{TA}}} \tag{4}$$

where b is the bias, c is a constant, and ξ is a standardised random variable. Given that the computational expense of a solution is proportional to $N_{TA} \times N_{PC}$, in order to minimize the error for a given computational cost one would prefer to use a higher value for N_{PC} and a lower value for N_{TA}. However computer memory limitations restrict how large one can choose N_{PC} (it directly affects file size). The procedure used here was to reach a statistically stationary initial solution with standard settings for both N_{TA} and N_{PC} (100 and 20 respectively). From this point, the maximum number of particles per cell is chosen for the capability of the resources available ($N_{PC} = 100$ for the test cases and $N_{PC} = 50$ for the lifted flame cases), and a uniform average is applied where the value of N_{TA} is increased by 1 for every iteration completed. The solutions for the diffusion terms are periodically checked for numerical noise, with fluctuating values less than around 10% of the maxima of the budget terms being acceptable. If the noise in the term is still greater than this threshold after a large number of iterations (e.g. 10 000) then noise filtering is applied to the fields.

2.6 *Noise filtering*

To reduce the noise in the plots, a noise filter was applied several times to the species transport budget results for the lifted flame cases. A five-point linear filter can be constructed to attenuate the value at x with data from surrounding values, spaced at an interval h, as equation (5)

$$\bar{f}(x) = af(x-2h) + bf(x-h) + (1-2(a+b))f(x) + bf(x+h) + af(x+2h). \tag{5}$$

The Taylor series expansion [equation (6)) gives

$$\bar{f}(x) = f(x) + 4ah^2 f''(x) + bh^2 f''(x) + \cdots \tag{6}$$

So to construct a fourth-order filter, we set $b = -4a$. Further, choosing a and b to minimize the variance of the filtered function [equation (7))

$$\mathrm{var}(\bar{f}(x)) = \{2a^2 + 2b^2 + [1-2(a+b)]^2\}\mathrm{var}(f) \tag{7}$$

gives a five-point filter vector [−3/35, 12/35, 17/35, 12/35, −3/35].

This vector can be applied to the data along the line plot of values in post-processing, but is more effective when incorporating information from the 5 × 5 region around the data point. This is done by constructing a 5 × 5 matrix generated from the tensor product of the vector with itself. Data are taken along evenly spaced lines either side of the plot of interest and the filter is applied to every point along the line. To apply the filter multiple times, data need to be incorporated from locations successively further away from the data point. The grid spacing is only uniform in the x- and r- directions up to x/D = 25 and r/D = 10, so the use of this particular filter has been limited to that region.

To illustrate the effect of this filtering operation, figure 3(a) shows the raw data for the species transport budget terms for the hydrogen atom in the lifted flame case with a co-flow temperature of 1045 K, and figure 3(b) shows the result of applying the filter to these data eight times. Of note is that the maxima, minima, axis intersections and general profiles are not shifted or attenuated. The species transport budget data presented in this paper for the

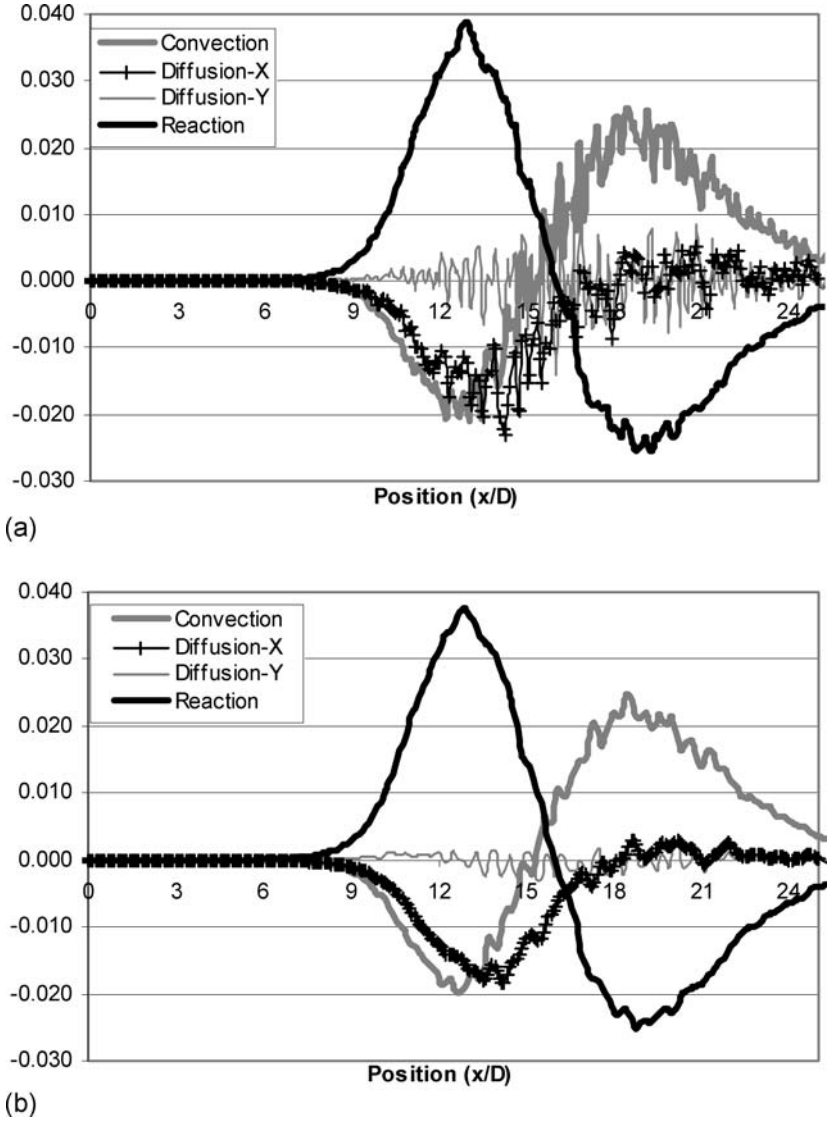

Figure 3. An example of the impact of the application of a fourth-order noise filter eight times to the species transport budget terms for the H intermediate for a lifted flame with a co-flow temperature of 1045 K. The profiles are taken along an axial line at r/D = 1.7. Note the unchanged magnitudes and locations of maxima/minima and axis intersections. (a) raw data; (b) filtered data.

lifted flames have been filtered eight times, except for the case with a co-flow temperature of 1080 K, where it has been applied six times (this is owing to not having enough data lines axially between the plot line and the axis to apply the filter more times, as the mean flame base lies closer to the axis than in the other two cases).

3. Lifted flames: general trends

Global features of these lifted flames such as lift-off heights, colour and noise have been studied experimentally for a range of conditions [24, 25]. For this burner geometry, the main

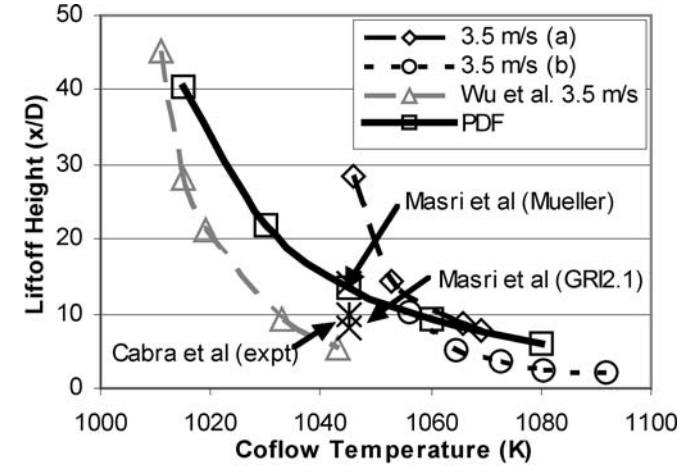

(a)

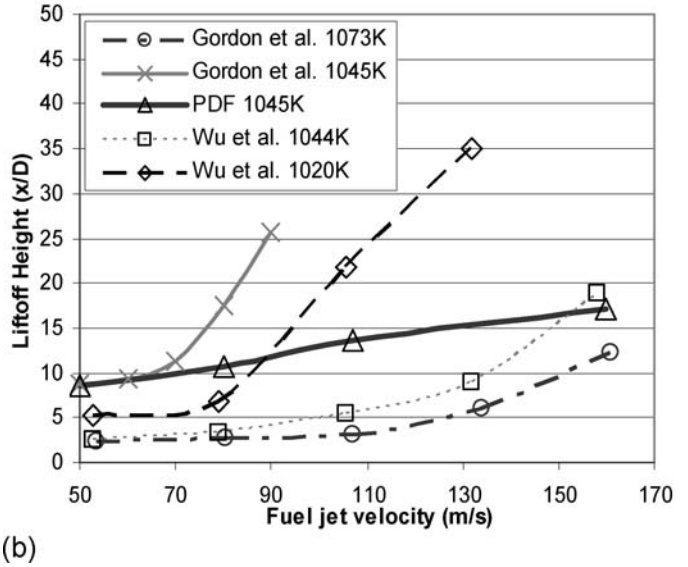

(b)

Figure 4. Lift-off height versus (a) co-flow temperature, and (b) fuel jet mean velocity for the lifted flame. Black solid line indicates results of the present calculations, which are compared to experimental data from Wu *et al.* [24] and Gordon *et al.* [25]. In (a), the Gordon *et al.* results for 3.5 m/s co-flow (a) and (b) indicate measurements taken from two separate experiments.

parameters controlling the flame characteristics are the temperature of the co-flow and the fuel jet velocity. Other parameters such as the velocity of the co-flow and the turbulence level in the co-flow are less influential. The lift-off height is defined, experimentally, as the average distance between the jet exit plane of the fuel pipe and the flame base where the luminescence is visible to the naked eye in a darkened room.

Figure 4(a) shows measurements of the lift-off height plotted with respect to the co-flow temperature for a given fuel jet velocity, $U_j = 107$ m/s. Initially, the lift-off height decreases significantly with increasing co-flow temperatures. Beyond this, the lift-off height is almost uniform and the flame remains very close to the burner's exit plane. This varying sensitivity of

the lift-off height with the co-flow temperature is interesting and may have implications as to whether the flame is stabilized through autoignition or partially premixed flame propagation. The lift-off height of the flame studied by Cabra *et al.* [8], as well as those of the flame calculated by Masri *et al.* [6] with two different chemical mechanisms, have been marked for reference. From the current calculations, the flame with a lift-off height of 10 diameters has a co-flow temperature of 1060 K. It is worth noting that the average measured Rayleigh temperature of the co-flow from the data available at [9] (taken at r = 30 mm) is 1058 K (RMS ~9 K), and that the adiabatic temperature for the co-flow is 1065 K.

As the accuracy of the relative temperature measurements within a single experimental run is around 0.1% (1 K), the shape of the response curve is an important test for modelling this flame configuration. The calculated lift-off heights show qualitatively similar behaviour to the experimental data, albeit with a shallower response gradient. The different marker used for lift-off height (which was defined numerically as the location of the maximum axial mean OH mass fraction gradient at the mean flame base) contributes only a 1 diameter discrepancy at $L_h = 10$ D, although the discrepancy at higher lift-off heights cannot be quantified owing to lack of data. However, the principal cause of the shallower response gradient appears to lie in the physical models. The lift-off height response curve calculated by Cao *et al.* [7] using joint velocity-turbulence frequency-composition PDF modelling matches the shape of the experimental data more closely. Other physical and chemical modelling issues that could impact on the shape and location of the response curve include:

i. chemical mechanisms: it is known that the flame is sensitive to the kinetic mechanism employed, as detailed in [6, 7]. In [6], the use of a different mechanism lowered the lift-off height by 6 diameters in the 1045 K co-flow case, and by 2–3 diameters in [7];
ii. the modelled PDF equation assumes gradient diffusion, which may not be physically accurate for this case.

There is little sensitivity in the results to the mixing model, shown by comparisons to the interaction by exchange with the mean (IEM) and Euclidean minimum spanning tree (EMST) models in showing a variation of around 1 diameter for the 1045 K co-flow case [7].

Absolute temperature measurements in this experiment may exhibit up to 3% error. The experimental data from [24] and [25] span this tolerance. At a lift-off height of 10 diameters, both experimental data points vary by 1.5% from the nominal co-flow temperature used in [8].

Figure 4(b) shows variations of the lift-off height with fuel jet velocity for a variety of co-flow temperatures. According to the experimental data the lift-off height increases almost linearly with increasing fuel jet velocity up to a point, and then increases more sharply. Further, the gradient of these responses increases with decreases in co-flow temperature. The linear variation of lift-off height with jet velocity is well known but the variation of the slope with the temperature of the co-flow and the increase in response gradient at different velocities are less clear and warrant further studies. The PDF model predicts a linear response to increased jet velocity within the velocity range and at the temperature considered.

Another study of the global characteristics of the same flame [24] includes measurements of the noise level, which seems to vary significantly between flames of low and high co-flow temperatures. Although these measurements are not resolved in spectral space, they consistently show that flames with low co-flow temperatures are noisy and fluctuating while those stabilized below x/D = 15 are quiet and stable. It has been conjectured [24] that noisy flames are indicative of the occurrence of auto-ignition (owing to the stabilization mechanism being a rapid series of loud auto-ignition events) while the quiet ones are lifted flames stabilized through partially premixed flame propagation. This, however, needs further investigation and may be answered through numerical experiments similar to those attempted here.

4. The indicators

It is clear from the studies reported earlier that the identification of auto-ignition is not straightforward and only inferences can be drawn from parameters such as lift-off height or flame noise. What is needed is a set of indicators that facilitate the distinction between auto-ignition and premixed flame propagation. This section attempts to perform such a task by identifying two possible indicators which are later tested and analyzed with respect to simple test cases as well as in the lifted flames. It is worth re-iterating here that some of the adopted indicators may be difficult, if not impossible, to test in the laboratory; hence the usefulness of the numerical experiments reported here.

4.1 *Indicator 1: species transport budgets of convection, diffusion and reaction (CDR budgets)*

In the simplest cases of auto-ignition, a balance is expected between reaction and convection with no contribution from diffusion. In contrast, the following trends are expected in premixed flames: a pre-heat zone, characterized by diffusion balancing convection while reaction is essentially zero; followed by the reaction zone, where the dominant balance is between reaction and diffusion away from the flame front, with convection having a minor role. It is important to make the distinction between axial and lateral diffusion both in the 2D premixed flame case as well as for the lifted flames.

At any point in the domain, the steady-state modelled transport equation [equation (8)] for the Favre mean mass fraction of species k is balanced by the three processes of convection, diffusion and chemical reaction

$$0 = -\frac{\partial}{\partial x_i}(\langle\rho\rangle\tilde{u}_i\tilde{Y}_k) + \frac{\partial}{\partial x_i}\left(\frac{\mu_T}{Sc_T}\frac{\partial\tilde{Y}_k}{\partial x_i}\right) + \langle\rho\rangle\tilde{S}_k \tag{8}$$

The first term on the right-hand side (RHS) of the equation represents convection (C) by the mean flow, the second term is turbulent diffusion (D), and the third is the reaction source term (R). Here, $\langle\rho\rangle$ is the mean density, $\tilde{u}_i$ is the Favre averaged velocity in the ith direction, $\tilde{Y}_k$ is the Favre averaged mass fraction of species k, μ_T is the turbulent viscosity, Sc_T is the turbulent Schmidt number, and $\tilde{S}_k$ is the chemical source term.

The directional components of the diffusion term are calculated separately to allow us to distinguish between axial diffusion (associated with premixed flame propagation) and radial diffusion (which may be present in auto-ignition stabilization). Since the mean flow direction immediately preceding and through the mean flame base is almost parallel to the x axis, the x and r components of diffusion approximate the streamwise and cross-stream components.

Each of the calculated terms is normalized by a factor of $\rho_J Y_{k,\max}/t_J$, where ρ_J is the density of the fuel stream, $Y_{k,\max}$ is the maximum mean species mass fraction for the species k over the whole field, and t_J is a representative time scale for the fuel flow. For the lifted flame cases, t_J is taken to be the jet diameter divided by the fuel bulk velocity; for the plug flow reactor, domain width divided by the inlet velocity; and for the premixed counterflow burner, twice the inlet width divided by the inlet velocity. The values of these factors are recorded in table 8.

4.2 *Indicator 2: 'time history' of radical concentrations*

The DNS studies of Echekki and Chen [17] show that with auto-ignition, the species HO_2 builds to an apparent critical threshold value prior to radical runaway and the initiation of

Table 8. Normalizing factors for CDR budgets.

Case	Normalizing factor for budget of		
	H_2O (excess)	H	HO_2
1D auto-ignition	296.8	0.183	0.197
2D Premixed	0.277	1.981×10^{-4}	2.486×10^{-4}
Lifted flame, $T_{coflow} = 1030$ K	735.4	0.207	1.227
Lifted flame, $T_{coflow} = 1045$ K	1173.6	1.454	1.639
Lifted flame, $T_{coflow} = 1080$ K	1438.9	5.315	1.513

ignition. If the build up of the radical is delayed (by high scalar dissipation, for instance) then the ignition delay is extended. For these steady state calculations considered here, following an axial path through the mean flame base can be considered as an approximation to the time history of the concentrations. The history of key flame radicals such as H, O, OH and HO_2 may be an indicator for the occurrence of auto-ignition whereby the latter may be characterized by a build up in the concentration of HO_2 prior to ignition while premixed flame propagation is characterized by the simultaneous initiation of build up of all radicals. These indicators are tested in the next section.

5. Validation of indicators

The indicators presented have been validated with respect to the test case for auto-ignition (which will be referred to as 1D auto-ignition) and the counterflow premixed case (which will be referred to as 2D premixed). A value of N_{TA} of 10 000 steps was needed to reduce fluctuations in the diffusion terms. Results are presented and discussed for each indicator separately.

Two constructed variables that are useful in analysing the detail of the reaction are excess temperature and excess water. These are defined as follows

$$T_{excess} = T - (T_{coflow}(1 - \xi) + T_{fuel}\xi) \tag{9}$$

$$Y_{H_2O,excess} = Y_{H_2O} - Y_{H_2O,coflow}(1 - \xi) \tag{10}$$

where ξ is the mixture fraction, calculated in these flows from the mass fraction of trace argon in the fuel ($\xi = Y_{Ar}/Y_{Ar,fuel}$). These expressions allow the analysis of the temperature rise or the fraction of water concentration that exists solely due to reactions, by removing the fraction owing to mixing. It is possible to analyse the species transport budget of excess H_2O by manipulating the equations for the convection and diffusion terms and substituting the definition for mixture fraction given above in terms of mass fraction of argon into equation (10) as follows

$$C_{Y_{H_2O,excess}} = C_{Y_{H_2O}} + C_{Y_{Ar}}(Y_{H_2O,coflow}/Y_{Ar,fuel}). \tag{11}$$

$$D_{Y_{H_2O,excess}} = D_{Y_{H_2O}} + D_{Y_{Ar}}(Y_{H_2O,coflow}/Y_{Ar,fuel}) \tag{12}$$

The reaction term in this formulation is identical to that for Y_{H_2O}.

It should be noted that equal diffusivities are assumed in the calculations, and so the mixture fraction based on each element is the same: argon is used for convenience. Also while, in the absence of reaction, species mass fractions and enthalpy are conserved variables, temperature is not. Hence there is a small contribution to T_{excess} owing to variations in specific heats.

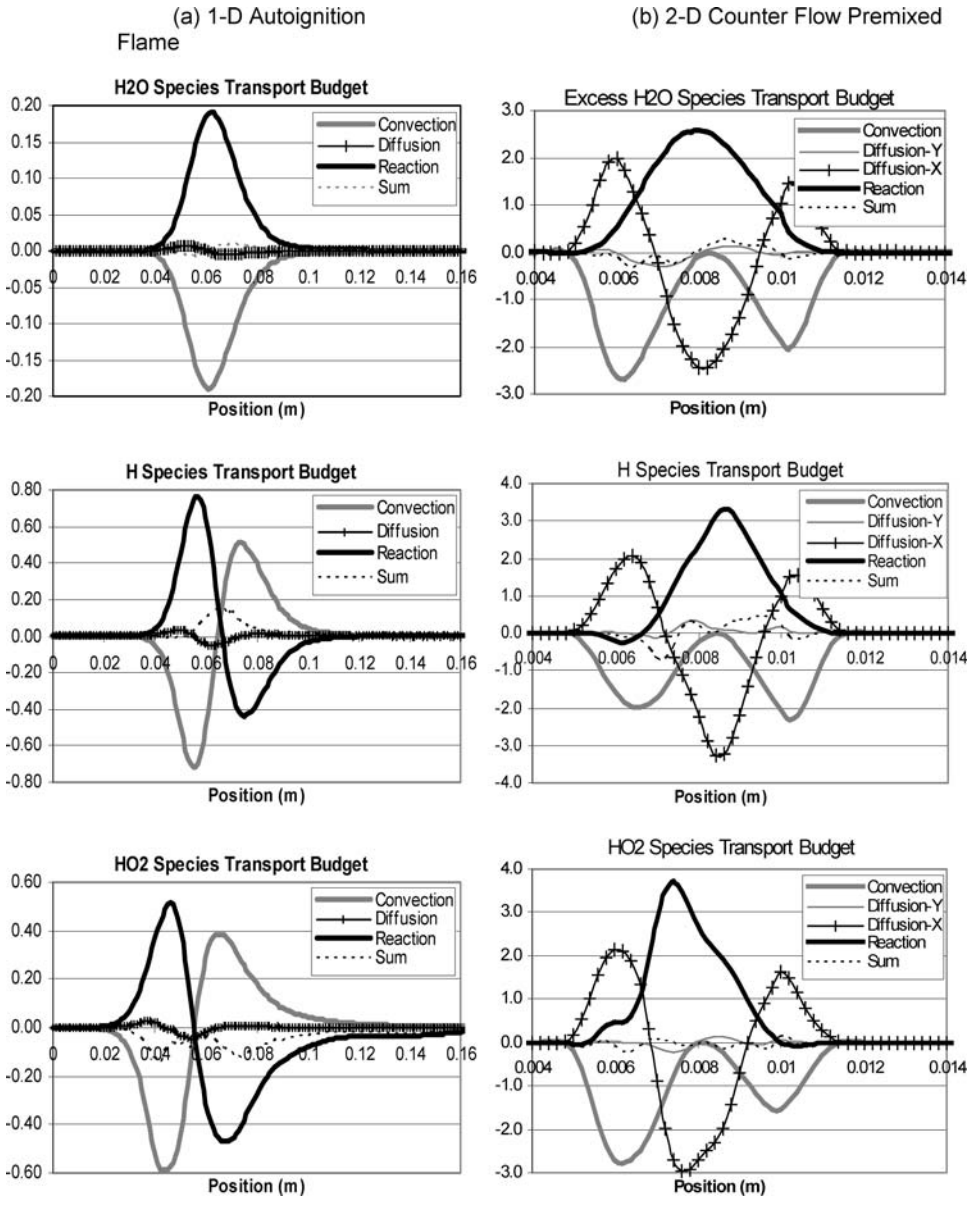

Figure 5. Species transport budgets of H_2O, H and HO_2 for (a) 1D auto-ignition along the centreline of the domain, and (b) 2D counterflow premixed flame along the symmetry plane. The sum of the budget terms is plotted as a thin dashed line.

5.1 *Indicator 1: species transport (CDR) budgets*

Figure 5 shows the CDR budgets of H_2O, H and $HO_2$for the 1D Auto-ignition case [left-hand side (LHS)) and for excess H_2O, H and HO_2 for the 2D premixed case (RHS) plotted versus distance. The budgets for the auto-ignition case show, as expected, that the dominant balancing terms are convection and chemical reaction. The diffusion term is an order of magnitude smaller and this is consistent for the three scalars studied here. Note that for the product, H_2O, there is

a single positive peak of the reaction term R, whereas for the intermediates, H and HO_2, there is first a positive peak, where the species are produced, followed by a negative peak where they are consumed. Plots on the RHS, which correspond to a premixed flame reveal a pre-heat zone that exists from x/D = 0.005 to 0.007 m, dominated by a convective-diffusive balance, followed by the reaction zone showing a balance between diffusion and reaction.

One of the key tests for the accuracy of the budget terms for each species is how close the sum of the terms is to zero. The sum of these terms is plotted on all budget graphs presented here. Because the calculations achieve a statistically stationary state, it follows that the CDR budget as implicitly evaluated in the particle method is in balance. Presumably, therefore, the observed imbalance arises because the three contributions presented in the figures have been evaluated differently than in the particle method. Specifically, any imbalance may be owing to splitting errors and spatial discretization errors in addition to statistical fluctuations.

5.2 *Indicator 2: time history of radical concentrations*

Figure 6 shows plots for the mean temperature and the mean mass fractions of HO_2, H, OH, O and H_2O_2 (normalized by their respective maxima) computed for the auto-ignition case (LHS) and the premixed flame case (RHS). In the auto-ignition case, the HO_2 radical builds up to a significant level prior to the runaway of ignition, and subsequently H, O and OH build

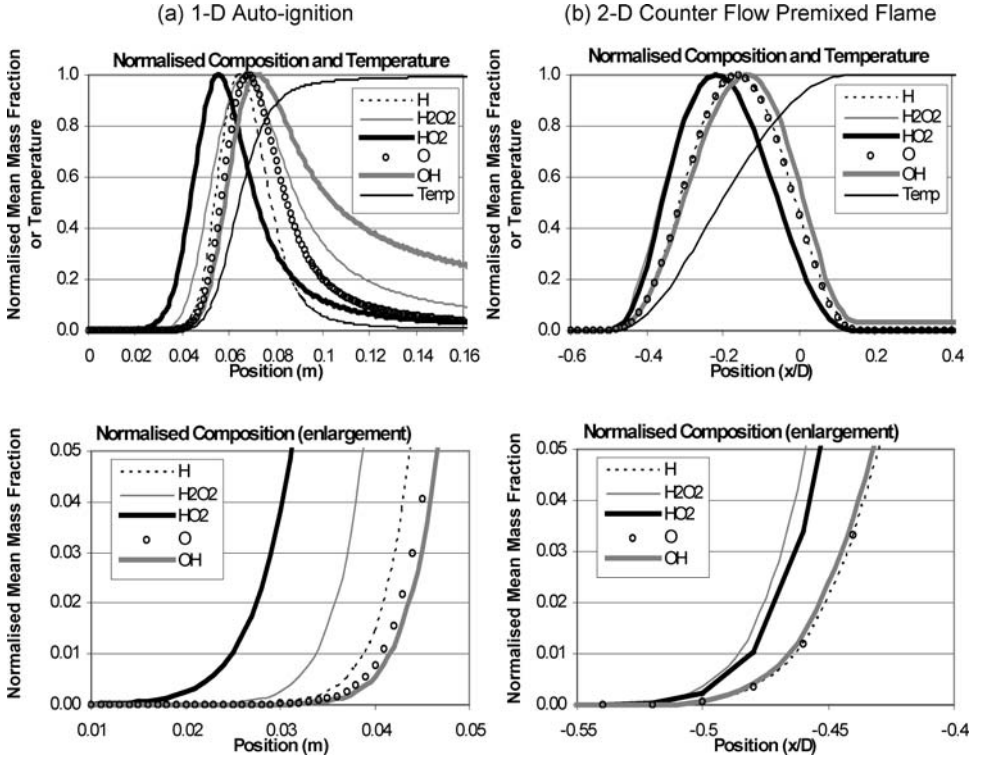

Figure 6. Normalized profiles of mean temperature, and mean mass fractions of the intermediates H, O, OH, H_2O_2, and HO_2 for (a) 1D auto-ignition along the centreline of the domain, and (b) 2D counterflow premixed flame along the symmetry plane. The bottom plots are enlargements of the mass fraction profiles at the initiation of species production.

up to significant levels. This may be contrasted with the premixed flame case in which the mass fractions of all the radicals begin increasing in the preheat zone at the same point. These results indicate that the onset of build up of HO_2 prior to other minor species such as OH, H and O is another relevant indicator for identifying the occurrence of auto-ignition.

6. Lifted flame results

The auto-ignition indicators discussed earlier are applied here to a range of flames selected from the conditions shown in figure 4(a). Three flames with a fuel jet velocity of 107 m/s and three different co-flow temperatures, $T_{coflow} = 1030$ K, 1045 K and 1080 K, are further investigated. In figure 4(a), these flames correspond, respectively, to the regions where the lift-off heights (i) are high and decreasing steeply (these flames are almost extinguished), (ii) have intermediate slope and (iii) are low and decreasing slowly with respect to increasing co-flow temperature.

In the calculations, the mean flame base is taken to be the most upstream location where the mean OH mass fraction first reaches 1×10^{-5}. All profiles are taken on a line axially through this location. The lift-off height is defined as the location of steepest axial gradient of mean mass fraction of OH along this line. In the flame stabilisation region, the O radical begins to be consumed before the OH radical, so is used as a marker for the end of the stabilisation reaction zone (see LHS of figure 7). The extent of this zone is taken to be the distance between the locations of 10% and 90% of the peak mean mass fraction of the O radical along the axial line. On the RHS of figure 7, this zone is superimposed on the mean mass fraction profiles of H_2O and excess H_2O, where the beginning of the zone corresponds to the onset of production of H_2O, and the end of the zone corresponds approximately to the peak gradient of excess H_2O mean mass fraction.

A comprehensive analysis of the mixing, temperature and composition fields for the base case relative to experimental data have been undertaken by Masri *et al.* [6]. For reference, experimental data along axial lines at r = 8 mm and r = 5.5 mm have been included in figures 7 and 8 for the 1045 K co-flow case. The first profile most closely matches the physical location of the calculated profiles, whereas the second profile is taken through the mean flame base of the experimental flame (as defined above) to account for the difference in mixing field predicted by the k–ε model. The data match well up to the lift-off height of the experimental flame. The lift-off height for the calculated flame is four diameters downstream of the experimental flame, explaining the remaining discrepancy.

Figure 8 shows axial profiles of mean mixture fraction, mean temperature, mean excess temperature and mean axial velocity for three flames. The axial profiles shown in each figure are taken at radial locations which coincide with mean flame base as defined earlier: $r/D = 3.0$ for the $T_{coflow} = 1030$ K case; $r/D = 1.7$ for the $T_{coflow} = 1045$ K case; and $r/D = 1.0$ for the $T_{coflow} = 1080$ K case. The boxed region on each plot shows the extent of the reaction zone at the flame base. These cases show lift-off heights (expressed in multiples of the fuel jet diameter, D) of approximately 22D, 13.5D and 7D respectively. Quantitatively different conditions exist at the mean flame bases of the three as shown in table 9, owing to the different axial and radial locations of these points, and the different co-flow temperatures.

The stoichiometric mixture fraction is 0.47, so the mixtures are quite lean at ignition. For the 1080 K co-flow case, the high excess temperature and the fact that the stabilization reaction region slightly precedes the temperature minimum indicate a very rapid initiation of the reaction. However, there is not enough information available in these data alone to draw conclusions about the nature of the stabilisation mechanisms for these flames.

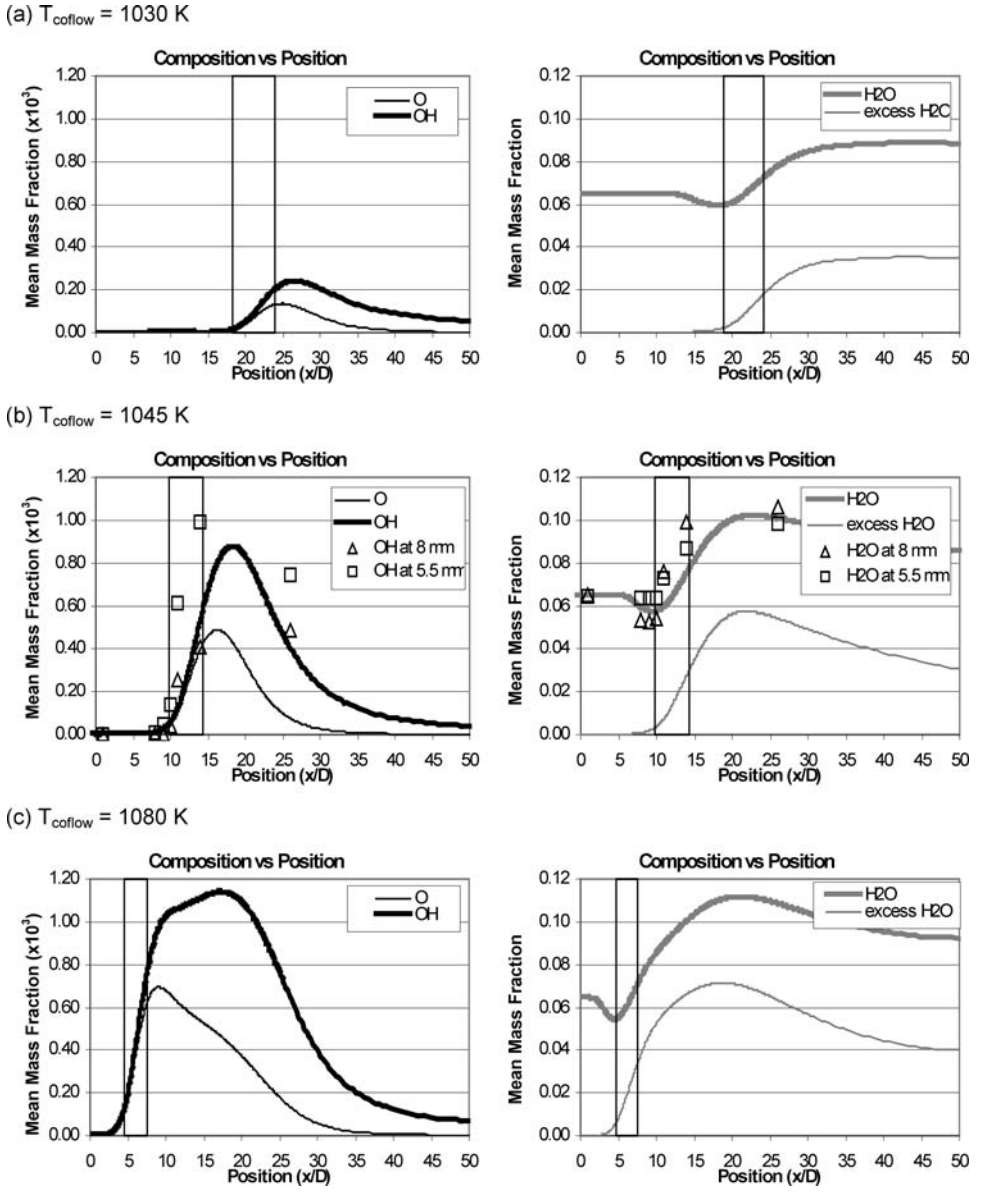

Figure 7. Mean species mass fractions of OH, O (LHS), H_2O and excess H_2O (RHS) for lifted flames with co-flow temperatures of (a) 1030 K, (b) 1045 K and (c) 1080 K. Plots are taken along r/D = 3.0, 1.7 and 1.0 respectively, being the axial lines that pass through the most upstream locations where the mean mass fraction of OH first reaches 1×10^{-5}, which is taken to be the mean flame base. Boxed regions denote the extent of the stabilization reaction zones, as defined by the region between the location of mean mass fractions of O between 10% and 90% of the peak mean O mass fraction along the plot line. Experimental data plotted on (b) are taken at r = 5.5 and 8 mm. 8 mm is the closest experimental data spatially to the profile plotted, while 5.5 mm corresponds to the radial location of the most downstream mean concentration of OH reaching 1×10^{-5}.

As mentioned earlier, the results for the CDR budgets for the flame cases have had noise filtering applied to maximise the quality of the signal information. The 1030 K and 1045 K co-flow cases have had the filter applied eight times, and the 1080 K case has had the filter applied six times.

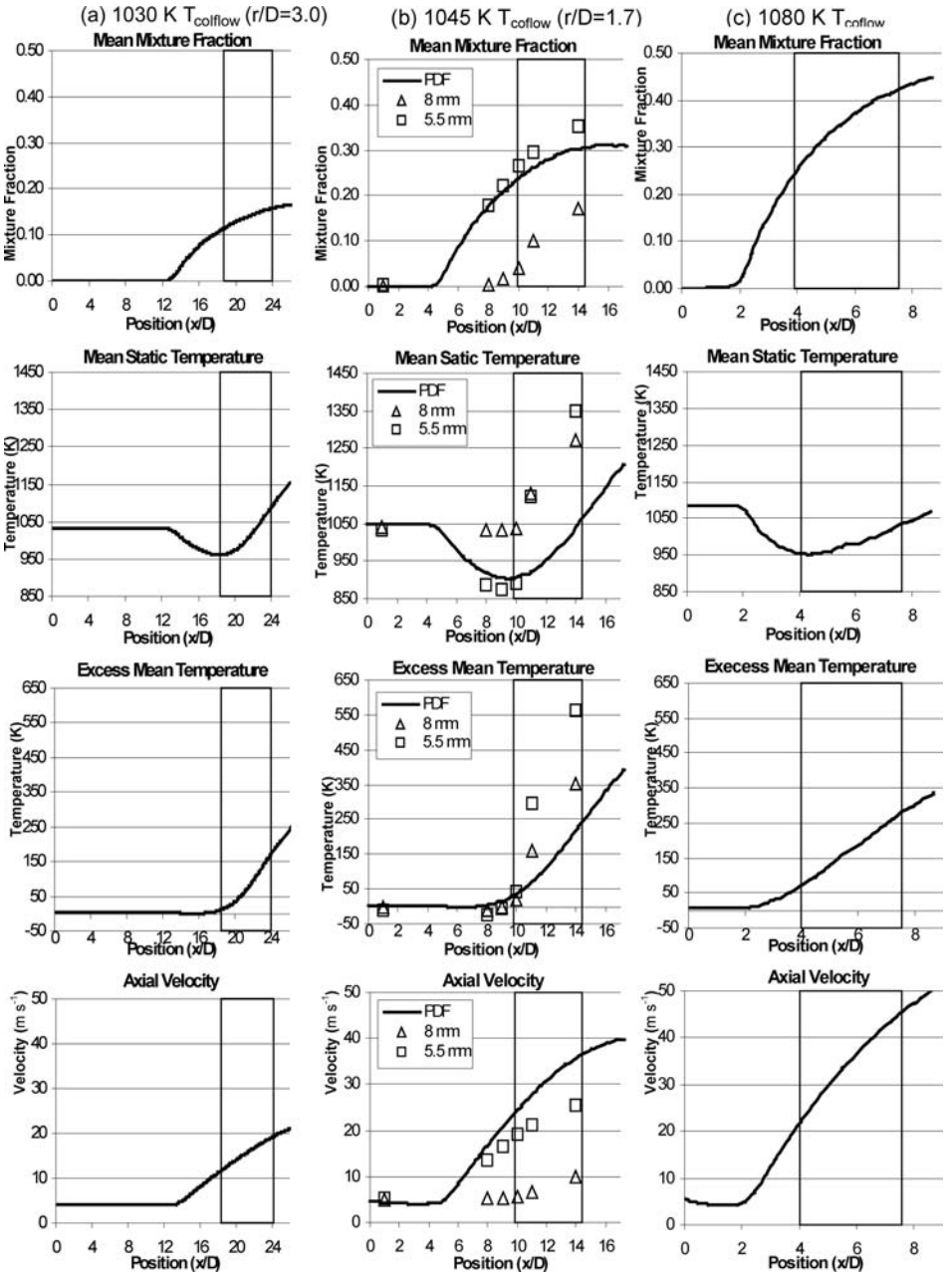

Figure 8. Axial plots of mixture fraction, mean temperature, excess temperature and velocity for lifted flames with co-flow temperatures of (a) 1030K T_{coflow} (r/D = 3.0); (b) 1045 K T_{coflow} (r/D = 1.7) (c) 1080 K T_{coflow} (r/D = 1.0). Boxed regions denote the extent of the stabilization reaction zones. Experimental data plotted on (b) are taken at r = 5.5 and 8 mm, as per figure 7.

6.1 *Indicator 1: CDR budgets*

As discussed previously, a rigorous test of the accuracy of the budget terms is whether the sum of C+D+R is zero as shown in equation (5). The sum is plotted on all budget figures (figure 9) as a thin dashed line. It is relevant to note here that when considering the CDR

Table 9. Conditions at mean flame base.

	Co-flow temperature		
Property	1030 K	1045 K	1080 K
Mean mixture fraction	0.11	0.24	0.26
Mean temperature	960 K	905 K	955 K
Mean excess temperature	9 K	37 K	73 K
Mean velocity	12 m/s	25 m/s	22 m/s

budgets of these flames, auto-ignition behaviour would be denoted by a convection-reaction balance, with *axial* diffusion being much smaller. Significant radial diffusion would still be expected in these cases.

Figure 9 shows axial profiles of convection, reaction and diffusion terms calculated at the radial locations described above for the three cases for excess H_2O, and the H and HO_2 radicals. The other species have been omitted here for brevity, as these plots display the characteristic information. The paths chosen allow one to approximate a temporal development of convection, diffusion and reaction through the middle of the mean flame base. Plots 9a, 9b and 9c refer, respectively, to the flames with $T_{coflow} = 1030$ K; $T_{coflow} = 1045$ K and $T_{coflow} = 1080$ K. Each flame is now analysed and discussed separately with respect to this indicator.

6.1.1 Case 1: $T_{coflow} = 1030$ K. This case was thought to represent a typical example of an auto-igniting flame which is fluctuating significantly at the stabilization base, noisy and very sensitive to the temperature in the co-flow. That the flame is auto-ignition stabilized is confirmed by CDR budgets [see figure 9(a)] for excess H_2O and the H radical that show a clear convective-reactive balance. Deeper in to the flame, radial diffusion of the H radical is observed. The HO_2 CDR budget exhibits a slightly more complex behaviour. The zone of interest for this radical species is immediately prior to the flame stabilization reaction zone, around x/D = 11 to 17, where first positive radial diffusion is balanced by convection, indicating a build up of the mass fraction through mixing from reactions that have taken place closer to the axis, and later positive reaction is balanced by convection, and radial diffusion goes negative–a balance which persists through the flame stabilization zone. Importantly though, the axial diffusion term is negligible. It is interesting to note the extent of the pre-flame reaction zone for HO_2 (nearly five jet diameters for the main pre-flame reaction), indicating extended auto-ignition delay times.

6.1.2 Case 2: $T_{coflow} = 1045$ K. This transitional case, chosen to match the conditions of the flame previously studied by Cabra *et al.* [7], also appears to be stabilized by auto-ignition. The excess H_2O CDR and H radical budgets [see figure 9(b)) are similar to that of the $T_{coflow} = 1030$ K flame and the plug flow reactor case, albeit with increased contributions from the radial diffusion term, which is almost as significant as the convective term in the H budget deep within the flame. The HO_2 CDR budget again shows an extended pre-flame reaction zone up to x/D = 10, consistent with the idea that HO_2 acts as a precursor to autoignition reactions in hydrogen chemistry. For all quantities, axial diffusion is negligible.

6.1.3 Case 3: $T_{coflow} = 1080$ K. Experimentally, this flame is quiet, stable and behaves like a standard lifted flame. One of the fundamental questions we seek to answer is: does the flame transition to one that is stabilized through partially premixed flame propagation, or is it stabilized through autoignition but with an extremely short delay? The CDR budgets in

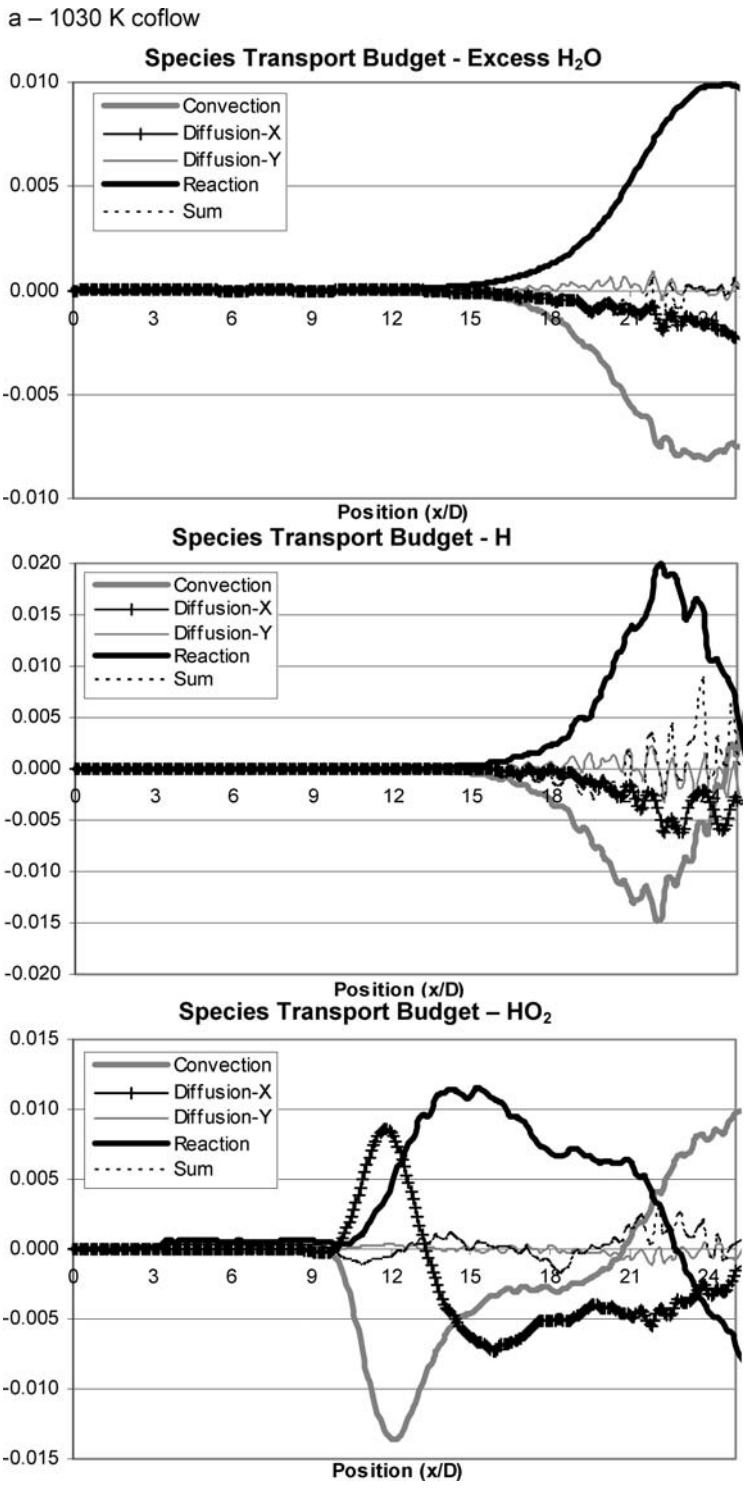

Figure 9. Species transport budgets of excess H_2O, H and HO_2 for lifted flames with co-flow temperatures of (a) 1030 K, (b) 1045 K, and (c) 1080 K. The sum of the budget terms is plotted as a thin dashed line. Data in (a) and (b) have had a fourth-order noise filter applied eight times, and data in (c) have had the filter applied six times. *(Continued)*

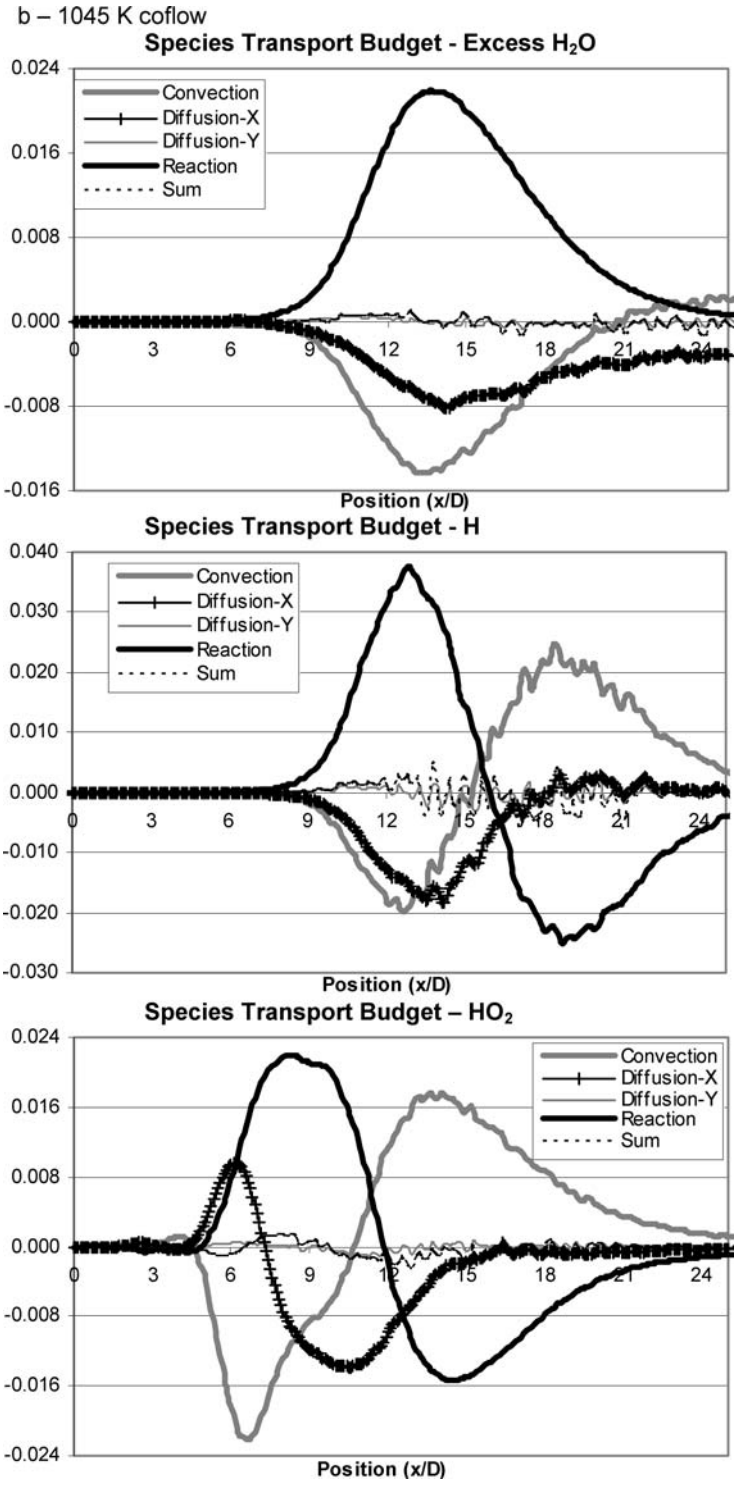

Figure 9. (Continued)

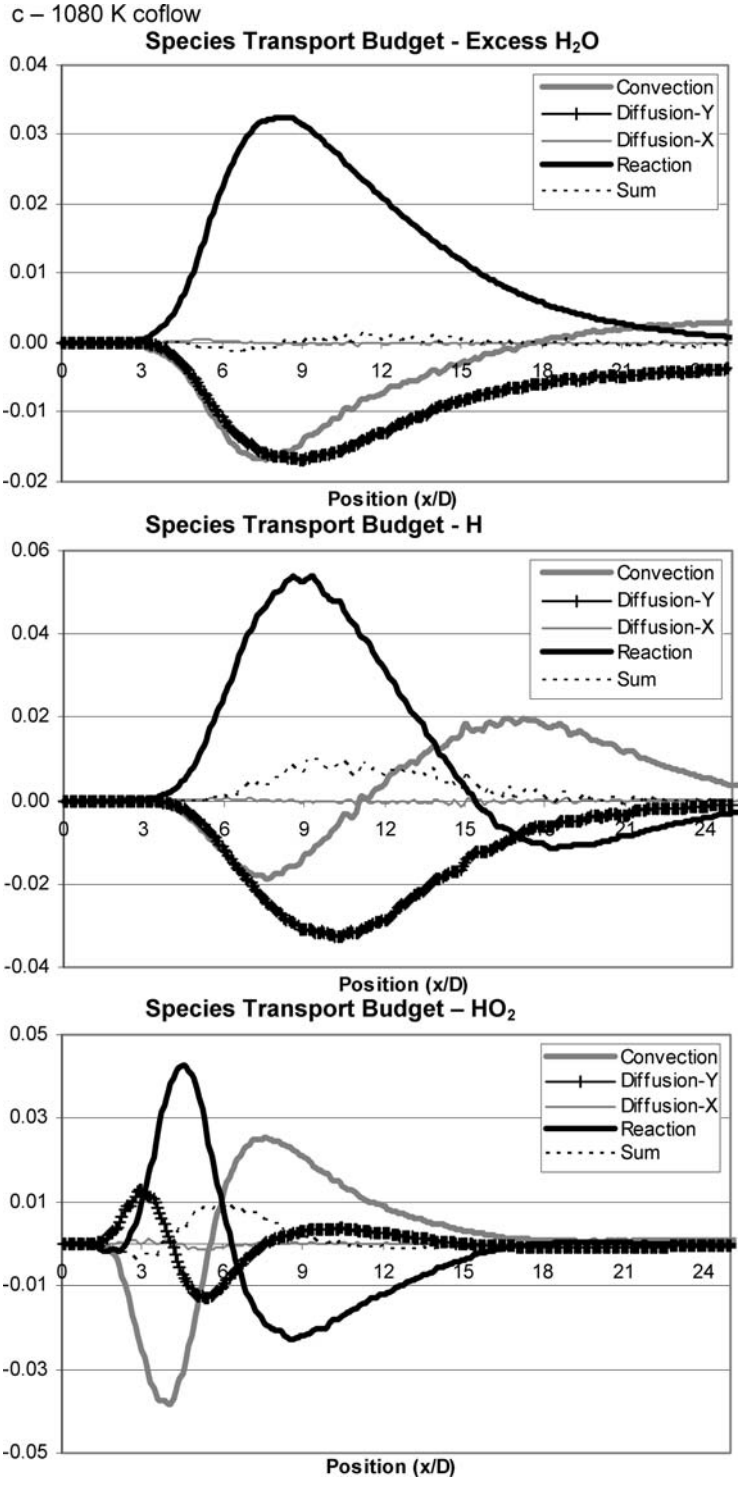

Figure 9. (Continued)

figure 9(c) indicate that the latter is the case, at least with respect to the calculations presented here. The axial diffusion term in all three budgets remains insignificant through the mean flame base. Radial diffusion of the H atom has increased in relative magnitude to being twice as large as the convective component of the budget deep within the flame, and begins at the onset of production of the radical. The results for the sum of terms for the radicals in this case exhibit a positive bias where the convection term changes sign. This is likely owing to the reasons discussed in section 5. Given the minimal axial diffusion, these results can be taken as an indication of auto-ignition stabilization for all three cases.

6.2 *Indicator 2: time history of radical concentrations*

Figure 10 shows the plots of the normalized mean mass fractions of HO_2, H, OH, O and H_2O_2 for the three flames. The RHS plots are magnifications of the mean flame base locations of each flame. Note that there is a non-zero mean mass fraction of OH upstream of the mean flame base. The mass fraction of OH reported by Cabra *et al.* [7] and used in these calculations for the pilot composition boundary condition is above equilibrium values at these temperatures. The mean OH mass fraction diminishes in the pilot stream upstream of the jet exit, reaching levels that, while still greater than equilibrium composition, are below the values that are considered to be the threshold for the stabilization reaction zone.

For the first two cases with co-flow temperatures of 1030 K and 1045 K, it is clear that HO_2 is being generated long before the reaction zone, and also that it begins to be consumed as soon as the production of H begins, consistent with its role as an auto-ignition precursor. The plot for the 1080 K co-flow case shows radical build up where HO_2 is generated only half a diameter upstream of the generation of OH and O, immediately upon mixing. It is, however, consumed at the onset of H production, a feature which is not present in the premixed flame test profiles.

7. Discussion

The results presented here are very encouraging in establishing a set of reliable indicators to further fundamental understanding of auto-ignition and premixed flame propagation. Both species transport budgets of convection, diffusion and reaction as well as the time history of radical concentrations are proving to be useful and complementary numerical tools. This has been clearly demonstrated in the two test cases of 1D plug flow reactor and 2D counterflow premixed burner.

Applying these indicators to the lifted flames with different conditions in the co-flow yields useful information about the mechanism of stabilisation. The flame with $T_{coflow} = 1030$ K shows a behaviour consistent with auto-ignition where a convective-reactive balance is obtained along with a build up of HO_2 radicals ahead of the reaction zone prior to ignition. These flames are also characterized by a high sensitivity to the temperature of the co-flow. A similar behaviour, indicative of auto-ignition also is noted for the flame with $T_{coflow} = 1045$ K. At higher co-flow temperatures (1080 K), the lift-off heights become much less sensitive to changes in temperature, but despite the qualitative indications that this flame may be stabilized through partially premixed flame propagation, the build up of HO_2 radicals prior to ignition is as distinct as for the previous cases. Further, the fact that there is no axial diffusion indicates that the $T_{coflow} = 1080$ K flame cannot be stabilized by flame propagation. It is reasonable that the high co-flow temperature is accelerating the reactive processes, and that the mixtures created will be auto-ignitable. For this flame to be stabilized by another mechanism, such a

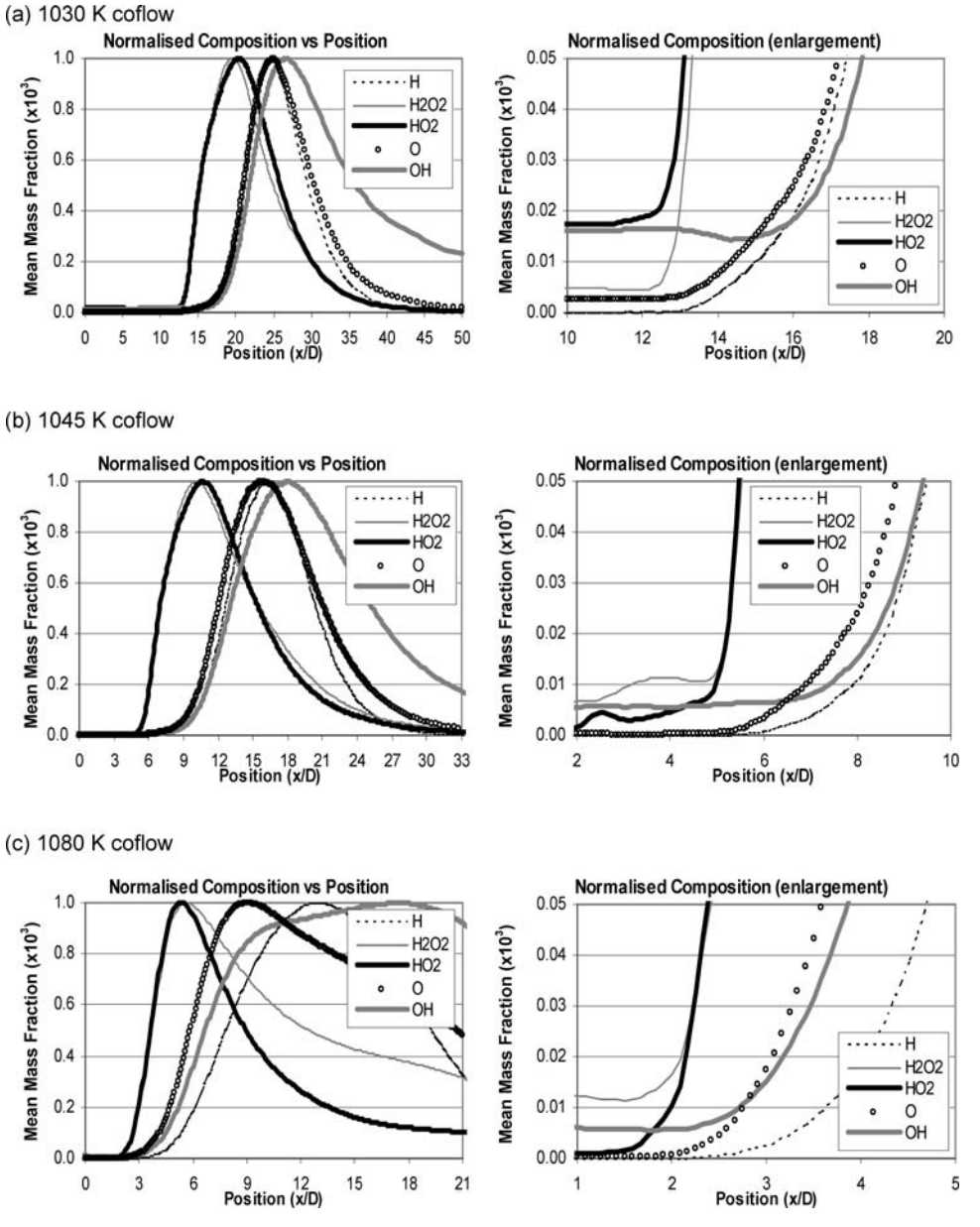

Figure 10. Normalized mean mass fractions of intermediates H, O, OH, H_2O_2 and HO_2 for lifted flames with co-flow temperatures of (a) 1030 K, (b) 1045 K, and (c) 1080 K. Plots on the RHS are enlargements of the region close to the mean flame base.

mechanism would need to be occurring faster than the ignition delay of the mixture, which would be apparent in the budgets.

These calculations employ a RANS–PDF method that uses the gradient diffusion hypothesis, relatively simple turbulence modelling, and has no account for differential diffusion effects. It has been shown that the methods employed here enable the capture of key features of the lifted flames in response to changes in co-flow temperature. The developed indicators are also able to distinguish between auto-ignition and premixed flame propagation and are identifying

auto-ignition in the lifted flames. It remains possible, however, that the flames with low lift-off heights observed at high co-flow temperatures are being stabilized by a mechanism not captured in these calculations.

The results of Cao *et al.* [7] also show that the use of more complex mixing models such as EMST make little difference in these flames confirming that they are largely controlled by chemical kinetics rather than by mixing. The results of Masri *et al*. and Cao *et al.* [6, 7] indicate that particular consideration will need to be given to the use of relevant chemistry mechanisms when flames of more complex fuels such as methane are considered. Reducing the noise to acceptable levels, particularly on the diffusion terms, will be a challenge and will require the efficient use of computational resources along with all the noise-reduction methods outlined in this paper. This is justified, however, given the relevance of these indicators and the valuable and unique information that result from such numerical experiments.

8. Conclusions

The hybrid RANS–PDF (Composition) approach is used here with detailed chemical kinetics to compute the structure of lifted flames of hydrogen–nitrogen fuel mixture issuing in a vitiated co-flow. The results agree well with experimental data with respect to the velocity and composition fields as well as with the variations of lift-off heights with co-flow temperature. Such good agreement is a necessary pre-requisite for using this hybrid approach as a tool for further numerical experiments.

Two numerical indicators are developed to distinguish between of flame stabilization by auto-ignition as opposed to stabilization through partially premixed flame propagation: (i) the budget of the convection, diffusion and reactive production of key species; and (ii) the qualitative behaviour of key radical species such as HO_2. The indicators successfully identify auto-ignition and premixed flame propagation in simple test cases. When applied to three selected turbulent lifted flames, they have provided information regarding the mode of stabilisation of all three flames that is indicative of auto-ignition stabilization.

These investigative tools show promise for furthering our understanding of the complex phenomena of auto-ignition and lifted flame stabilization. Further refinements in computing the indicators may be made through the use of improved sub-models as well as better noise reduction methods. This paper, however, establishes clearly that the trend of using numerical experiments to probe difficult and experimentally hostile combustion issues is now possible and can only broaden as numerical capabilities continue to improve.

Acknowledgements

This work is supported by the Australian Research Council and the US Air Force Office of Scientific Research Grant No. F49620-00-1-0171. Aspects of this research were conducted using the resources of the Cornell Theory Center, which receives funding from Cornell University, New York State, federal agencies, foundations, and corporate partners.

References

[1] Tang, Q., Xu, J. and Pope, S.B., 2000, Probability density function calculations of local extinction and NO production in piloted-jet turbulent methane/air flames, *Proceedings of Combustion Institute*, **28**, 133–140.

[2] Lindstedt, R.P., Louloudi S.A. and Vaos, E.M., 2000, Joint scalar probability density function modeling of pollutant formation in piloted turbulent jet diffusion flames with comprehensive chemistry, *Proceedings of Combustion Institute*, **28**, 149–156.

[3] Lindstedt, R.P. and Louloudi, S.A., 2002, Joint scalar transported probability density function modelling of turbulent methanol jet diffusion flames, *Proceedings of Combustion Institute*, **29**, 2147–2154.

[4] Liu, K., Pope, S.B. and Caughey, D.A., 2005, Calculations of bluff-body stabilized flames using a joint probability density function model with detailed chemistry, *Combustion and Flame*, **141**, 89–117.
[5] Masri, A.R., Pope, S.B. and Dally, B.B., 2000, Probability density function computations of a strongly swirling nonpremixed flame stabilized on a new burner, *Proceedings of Combustion Institute*, **28**, 123–132.
[6] Masri, A.R., Cao, R., Pope, S.B. and Goldin, G.M., 2004, PDF calculations of turbulent lifted flames of H_2/N_2 fuel issuing into a vitiated co-flow, *Combustion Theory Model*, **8**, 1–22.
[7] Cao, R., Pope, S.B. and Masri, A.R., 2005, Turbulent lifted flames in a vitiated coflow investigated using joint PDF calculations, *Combustion and Flame*, **142**, 438–453.
[8] Cabra, R., Myrvold, T., Chen, J.Y., Dibble, R.W., Karpetis, A.N. and Barlow, R.S., 2002, Simultaneous laser Raman-Rayleigh-LIF measurements and numerical modeling results of a lifted turbulent H_2/N_2 jet flame in a vitiated coflow, *Proceedings of Combustion Institute*, **29**, 1881–1888.
[9] Cabra, R., http://www.me.berkeley.edu/cal/VCB/ accessed 3rd November, 2003.
[10] Mastorakos, E.T.A., Baritaud, B. and Poinsot, T.J., 1997, Numerical simulations of autoignition in turbulent mixing flows, *Combustion and Flame*, **109**, 198–223.
[11] Mastorakos, E.T.A., da Cruz, T.A., Baritaud, B. and Poinsot, T.J., 1997, A model for the effects of mixing in the autoignition of turbulent flows, *Combustion Science Technology*, **125**, 243–282.
[12] Sreedhara, H. and Lakshmisha, K.N., 2000, Direct numerical simulation of autoignition in a non-premixed, turbulent medium, *Proceedings of Combustion Institute*, **28**, 25–34.
[13] Sreedhara, H. and Lakshmisha, K.N., 2002, Autoignition in a non-premixed medium: DNS studies on the effects of three-dimensional turbulence, *Proceedings of Combustion Institute*, **29**, 2051–2059.
[14] Sreedhara, H. and Lakshmisha, K.N., 2002, Assessment of conditional moment closure models of turbulent autoignition using DNS data, *Proceedings of Combustion Institute*, **29**, 2069–2077.
[15] Hilbert, R. and Thevenin, D., 2002, Autoignition of turbulent non-premixed flames investigated using direct numerical simulations, *Combustion and Flame*, **128**, 22–37.
[16] Hilbert, R., Tap, F., Veynante, D. and Thévenin, D., 2002, A new modeling approach for the autoignition of a non-premixed turbulent flame using DNS, *Proceedings of Combustion Institute*, **29**, 2079–2085.
[17] Echekki, T. and Chen, J.H. 2003, Direct numerical simulation of autoignition in nonhomogeneous hydrogen-air mixtures, *Combustion and Flame*, **134**, 169–191.
[18] Chen, J.H., Hawkes, E.R., Sankaran, R., Mason, S.D. and Im, H.G., 2006, Direct numerical simulation of ignition front propagation in a constant volume with temperature inhomogeneities: I. Fundamental analysis and diagnostics, *Combustion and Flame*, **145**, 128–144.
[19] de Charentenay, J., Thévenin, D. and Hilbert, R., 2003, Analysis of the stabilization processes of detached non-premixed flames, *Proceedings of the European Combustion Meeting ECM03,* Orléans (France), pp. 132/1–132/6.
[20] Mueller, M.A., Kim, T.J., Yetter, R.A. and Dryer, F.L., 1999, Flow reactor studies and kinetic modeling of the H_2/O_2 reaction, *International Journal of Chemical Kinetics*, **31**, 113–125.
[21] Pope, S.B., 1997, Computationally efficient implementation of combustion chemistry using in situ adaptive tabulation, *Combustion Theory Model*, **1**, 41–63.
[22] Incropera, F.P. and DeWitt, D.P., 2002, *Fundamentals of Heat and Mass Transfer*, 5th edition (New York: Wiley), p. 907.
[23] Cheng, R.K. and Oppenheim, A.K., 1984, Autoignition in methane-hydrogen mixtures, *Combustion and Flame*, **58**, 125–139.
[24] Wu, Z., Stårner, S.H. and Bilger, R.W., 2003, Lift-off heights of turbulent H_2/N_2 jet flames in a vitiated coflow, In: D. Honnery (Ed) *Proceedings of the 2003 Australian Symposium on Combustion and the 8th Australian Flame Days*, Monash University, Australia.
[25] Gordon, R.L., Stårner, S.H., Masri, A.R. and Bilger, R.W. 2005, Further characterisation of lifted hydrogen and methane flames issuing into a vitiated coflow, *Proceedings of the 5th Asia-Pacific Conference on Combustion,* University of Adelaide, pp. 333–336.